# Atomic force microscopy of (100), (110), and (111) homoepitaxial diamond films

L. F. Sutcu, C. J. Chu,[a] M. S. Thompson,[b] R. H. Hauge,[a] J. L. Margrave,[a] and M. P. D'Evelyn

*Department of Chemistry and Rice Quantum Institute, Rice University, Houston, Texas 77251-1892*

We present atomic force microscopy images of diamond films grown by chemical vapor deposition epitaxially on diamond (100), (110), and (111) substrates. The films were grown from 0.2%–1.6% mixtures of $CH_4$ and $C_2H_2$ in $H_2$ in a hot-filament reactor at a total pressure of 25 Torr. The substrate and filament temperatures were held at 810–1000 and 2000–2150 °C, respectively. A (100)-oriented diamond film grown with 0.3% $CH_4$ at a substrate temperature of 810 °C was rough on the $\mu$m scale, exhibiting pyramidal features, terraces, and penetration twins, while films grown at higher substrate temperatures and hydrocarbon flow rates were smooth on the nm scale and showed evidence of a $(2 \times 1)$ reconstruction. A (110)-oriented film was very rough on the $\mu$m scale but nearly atomically smooth on the 0.5–5 nm scale and exhibited local slopes higher than 40° with no evidence of faceting. A film grown on a diamond (111) substrate underwent spontaneous fracture due to tensile stress and exhibited a roughness of $\approx$10–50 nm on the $\approx$100 nm lateral scale in regions far away from any cracks. The implications of the morphological features for diamond growth mechanisms are discussed.

## I. INTRODUCTION

The extreme properties of diamond and the myriad of applications for diamond thin films have motivated the rapid growth of chemical vapor deposition (CVD) growth technology. For electronic applications in particular there is great interest in growth of high-quality single-crystal diamond films, and diamond homoepitaxy has been achieved by many research groups.[1-11] Homoepitaxial growth studies also promise to be extremely useful in advancing our level of understanding of the growth mechanism(s). Although much has been learned about the gas-phase chemistry in hot-filament CVD environments[12-14] and several detailed models of diamond growth have been proposed,[15-20] virtually nothing is known about the details of the decomposition of $CH_x$ intermediates on the growing surface. Characterization of film morphologies on the near-atomic scale may help elucidate some of these growth details, and may be useful as well in better understanding nucleation and the factors that control morphology on the micrometer scale.

Electron microscopy has been by far the dominant tool for the morphological characterization of diamond films. However, scanning tunneling microscopy (STM) and atomic force microscopy (AFM) routinely achieve atomic resolution on many substrates, and seem much better suited to the determination of the nanometer-scale structure of diamond films. Several groups have applied STM to the characterization of B-doped and undoped polycrystalline diamond films,[21-25] but only a limited resolution has been achieved to date. Near atomic-level resolution has

recently been achieved by Tsuno *et al.* by STM on a homoepitaxial (100) diamond film.[26] The need for electrically conducting substrates for STM appears to be a serious limitation for the characterization of diamond films, and AFM, which has no such requirement, would seem to be a more generally applicable tool. The ability to characterize undoped films is particularly important because boron doping has been shown to change the surface morphology of diamond films.[4,25] However, early AFM images of polycrystalline diamond films[25,27] have been limited to a resolution of $\approx$30 nm.

In this study, we have examined the surface topography of homoepitaxial diamond films grown by hot-filament CVD on (100)-, (110)-, and (111)-oriented natural diamond single-crystal substrates by AFM. A preliminary account of this work has been reported previously.[28]

## II. EXPERIMENTAL

Homoepitaxial diamond films were grown by hot-filament CVD in a reactor that has been described in detail previously.[9,13(a)] The filaments consisted of six strands of 0.13-mm-diameter tungsten wire approximately 10 mm in length which were resistively heated. The single-crystal, type 2A natural diamond substrates, obtained from Dubbeldee Harris, were $1.5 \times 1.5$ mm$^2$ in area and 0.1 mm thick, and were placed in a foil heater situated $\approx$9 mm below the filament after rinsing with acetone. The temperatures of the filament and samples were measured by an optical pyrometer and a Pt/Pt-13% Rh thermocouple, respectively. The total pressure in the reactor was held at 25 Torr during each deposition. A total of five films were analyzed in this study; the experimental growth conditions used for each sample are tabulated in Table I. Hydrogen was introduced above the filament and hydrocarbon gas(es) were injected between the filament and sample

TABLE I. Experimental conditions for growth of homoepitaxial diamond films characterized by atomic-force-microscopy.

| | Diamond samples (type 2A substrates) | | | | |
| --- | --- | --- | --- | --- | --- |
| | I | II | III | IV | V |
| Substrate orientation | (100) | (100) | (100) | (110) | (111) |
| Substrate growth temperature (°C) | 810 | 850 | 1000 | 850 | 966 |
| Film thickness ($\mu$m) | 2.9 | 2 | 12 | 5.1 | 9.2 |
| Substrate heater (0.06-mm-thick foil) | Mo | Pt | Pt | Pt | Pt |
| $H_2$ flow (sccm, over filaments) | 168 | 179 | 176 | 179 | 152 |
| $H_2$ flow (sccm, with hydrocarbons)[a] | 10 | 11 | 10 | 11 | ⋯ |
| $CH_4$ flow (sccm)[a] | 0.5 | 0.3 | 3 | 0.3 | 0.3–1.3 |
| $C_2H_2$ flow (sccm)[a] | 0.00 | 0.15 | 0.00 | 0.15 | 0.00 |
| Filament temperature (°C) | 2010 | 2000 | 2125 | 2000 | 2160 |

[a]Introduced below the tungsten filaments [Ref. 13(a)] except in the case of sample V, which was introduced over the filaments.

during growth of samples I–IV, as described previously.[9,13(a)] Both the hydrogen and hydrocarbon were introduced above the filament during growth of sample V. A mixture of $^{13}CH_4$ and $^{12}CH_2H_2$ was used in growing samples II and IV, while unlabeled methane was used for samples I, III, and V. Sample V, with a total film thickness of 9.2 $\mu$m, was used in a study of homoepitaxial growth kinetics, as reported elsewhere.[29] The $CH_4$ flow rate was varied from 0.3 to 1.3 sccm, corresponding to hydrocarbon mole fractions of 0.2–0.85%. The final growth step for sample V employed 0.6 sccm (0.3%) $CH_4$ and yielded a 1.0-$\mu$m-thick film.

AFM images were obtained in ambient air using a Digital Instruments Nanoscope II AFM utilizing an optical lever in combination with a microfabricated $Si_3N_4$ tip and cantilever. The AFM was operated in the repulsive force mode. Typical forces between the sample and the tip were in the range of $10^{-6}$–$10^{-8}$ N. Most AFM images of samples were acquired within a few weeks after their growth. Several samples were later re-scanned by AFM (images not shown) following treatment in boiling, concentrated sulfuric acid to remove graphite and other impurities. The appearance of surface features was very similar, as discussed below, but the amount of unidentified debris increased slightly.

The samples were also characterized by Raman spectroscopy, using a Spex Raman spectrometer and 514 nm (2.41 eV) $Ar^+$ laser excitation. Film thicknesses were determined by analysis of the fringe patterns in transmission Fourier-transform infrared spectra.[9]

## III. RESULTS

Raman spectra of samples I–IV are shown in Fig. 1. The Raman spectrum of sample I, shown in Fig. 1(a), shows the sharp first-order Raman peak of diamond at 1332 cm$^{-1}$ and no evidence of a graphitic feature near 1550 cm$^{-1}$.[30–32] The signal intensity in this spectrum was lower than that in spectra obtained from other samples, presumably due to scattering caused by the roughness of the surface, and the amplitude has been multiplied by ten in order to better show the base line. The 1332 cm$^{-1}$ peak in Fig. 1(a) contains contributions from both the substrate and the film, based on a comparison with micro-Raman

spectra (not shown). Micro-Raman spectra obtained from different regions of sample I were nearly identical and very similar to Fig. 1(a), albeit with a smaller 1332 cm$^{-1}$ peak. The shoulder on the high-frequency side of the 1332 cm$^{-1}$ peak has been observed previously in polycrystalline diamond films[32] and may be due to defects, but is probably not due to amorphous or graphitic carbon since it should have been accompanied by a more intense peak near 1550 cm$^{-1}$.[30–32]

The Raman spectra of samples II, III, and IV, shown in Figs. 1(b), 1(c), and 1(d), respectively, similarly show no evidence of graphitic carbon, and also no indication of a high-frequency shoulder on the 1332 cm$^{-1}$ peak. As samples II and IV comprise 57%-$^{13}$C/33%-$^{12}$C films,[13(b)] the Raman fundamental of the diamond film occurs at 1300 cm$^{-1}$ and is distinct from the peak due to the substrate. Unfortunately, sample V was lost after acquisition of the AFM images and we were unable to obtain its Raman spectrum. However, all homoepitaxial (111) diamond films that we have grown have a small-amplitude, broad Raman peak near 1550 cm$^{-1}$, indicating graphitic inclusions, as reported previously,[9] and this was presumably also true for sample V.
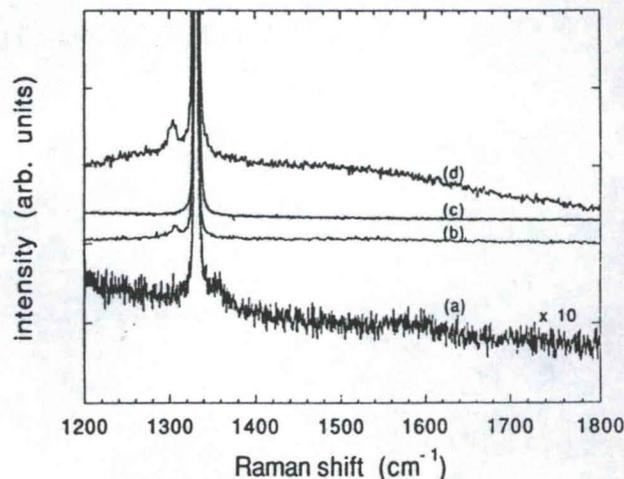


FIG. 1. Representative Raman spectra of (a) sample I, (b) sample II, (c) sample III, and (d) sample IV.
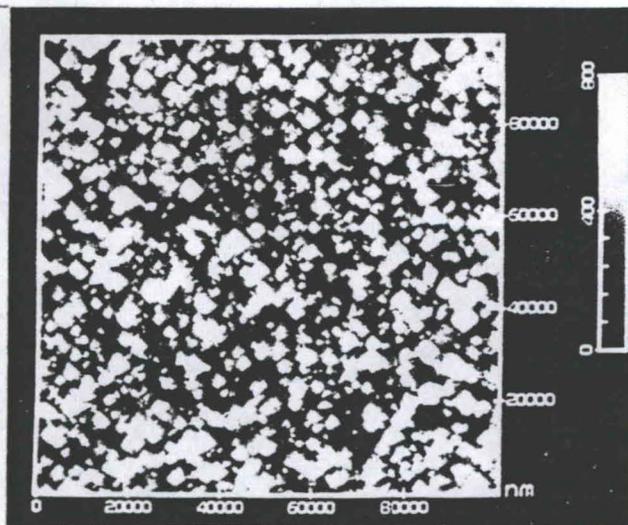
FIG. 2. $100 \times 100 \ \mu m^2$ AFM scan of epitaxial diamond (100) film (sample I).



(a)



(b)

FIG. 3. Three-dimensional views of pyramids and penetration twins on the faceted (100) surface (sample I): (a) $20 \times 20 \ \mu m^2$ scan, showing flat-topped pyramids; (b) $11 \times 11 \ \mu m^2$ scan, showing ledge structure.

A large area $(0.1 \times 0.1 \ mm^2)$ AFM image of sample I is shown in Fig. 2. The film surface is very rough and faceted, comprising square pyramidal features and sharper triangular features with a total height variation of $\approx 0.8$ $\mu m$. Both the pyramidal and triangular features follow the square orientation of the (100) substrate, with the triangular features being rotated by $\pm 90°$ or $180°$ at random about a principal axis direction. The larger pyramidal features are observable with an optical microscope, proving that the morphology observed by AFM is not an artifact resulting from tip effects. The pyramids are typically 5000–7000 nm wide and 200–300 nm high. Micro-Raman spectra obtained from the pyramids, triangular features, and areas in between the pyramids were nearly identical and very similar to Fig. 1(a), indicating that all of the features are high-quality diamond. Two higher resolution images of portions of sample I are shown in Fig. 3. Some of the pyramids on sample I have smooth sides, while those visible in Fig. 3 show a clear terraced structure with ledges. Some pyramids have ledges 500–1500 nm wide. On some of the pyramids the sloped sides extend up to the top, whereas other pyramids have flat tops, with widths of 500–2000 nm. Typical slopes of the sides of the pyramids and of the regions between ledges are $\approx 5°$ (the vertical scale in Fig. 3 is expanded). Assuming that steps are one atom high (1/4 lattice constant), the $5°$ slope implies a (100) terrace width of $\approx 10$ Å. Sample I was re-scanned by AFM after being boiled overnight in concentrated sulfuric acid, but no changes in the surface features and roughness were observed by AFM after the procedure. We were unable to achieve near-atomic-level resolution on this sample, but with the exception of the tops of the triangular features, the film [near-(100) orientation] was *locally* very smooth, with a roughness on the 1–100 nm scale less than 5 nm in amplitude.

The sharp triangular features seen in Figs. 2 and 3 (which appear dark in Fig. 3) are much rougher than the
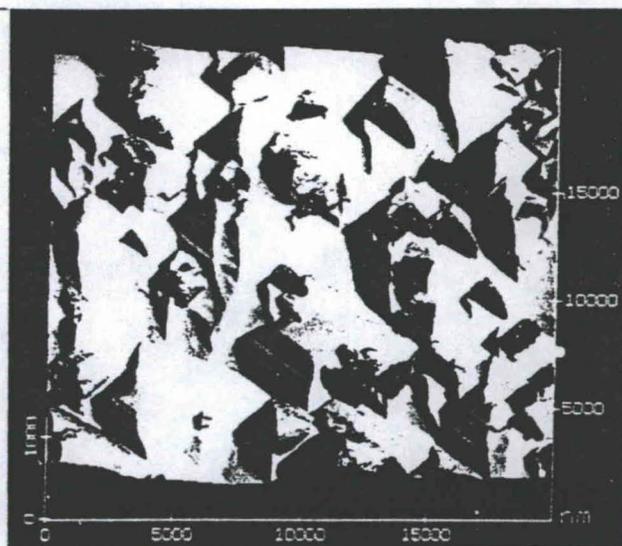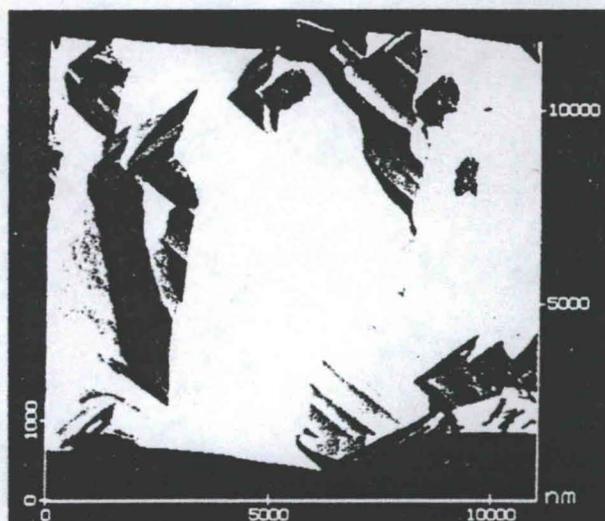
pyramids in appearance, are typically 400–1000 nm wide and 100–300 nm high, and are identified as penetration twins.[33] They appear to be more or less randomly distributed with respect to the pyramids. Figure 4 shows an isolated penetration twin, also on sample I. The penetration twins typically have one rough, gently sloping face and two steeper, smooth faces exposed. The rough faces are almost certainly of (111) orientation, as their morphology is qualitatively identical to that we observe in (111) homoepitaxial films but quite different from that of (100)-oriented films, and only (111) and (100) facets are normally observed in polycrystalline diamond films. The assignment of the triangular features as penetration twins follows from the angle between the normal to the rough face and ⟨100⟩ (the substrate normal), typically $15°$–$20°$. This value is much smaller than the angle between ⟨111⟩ and ⟨100⟩ within bulk diamond, $54.7°$, which implies the existence of subsurface twin planes beneath the triangular features. The

FIG. 6. Three-dimensional AFM image of epitaxial (100) diamond (sample III) with adsorbed contaminants.
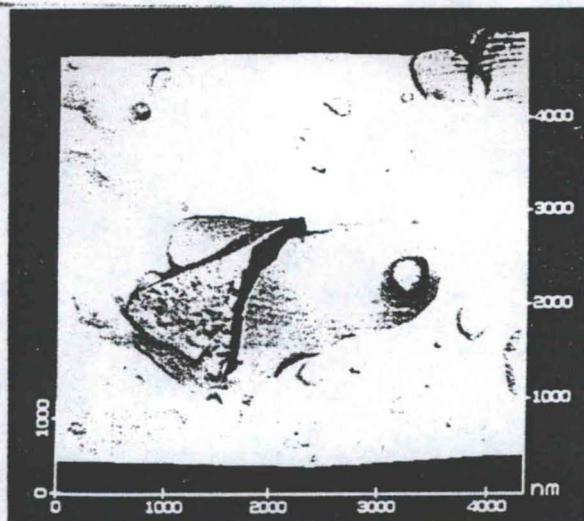
FIG. 4. Three-dimensional view of an isolated penetration twin on the faceted (100) surface (sample I).

steep sides of the penetration twins make a much sharper angle with respect to the substrate, $\approx 40°-50°$. This latter value may underestimate the true angle as the AFM image is essentially a convolution of the shapes of the sample and tip and we do not know precisely how sharp the AFM tip was. The smoothness of the steep sides of the penetration twins suggests that they are of (100) orientation. Nearly identical features were observed on (100) faces of cubo-octahedral diamond crystals by Clausing et al.,[34] who similarly identified the rough surface of the penetration twin as being (111) oriented and the smoother sides as (100) facets. The angle made by the intersection of the two steep sides with the rough face is $\approx 30°$. This value is much smaller than the ideal value of 60° for the intersection of (111) planes with (100) and (010) planes, which in turn implies the existence of a vertically oriented twin plane in the middle of the triangular features in addition to the subsurface twin.

Figure 5 shows an AFM line plot of sample II, which



FIG. 5. AFM image of epitaxial (100) diamond film (sample II).

was grown at a slightly higher temperature than samp The surface is seen to be fairly smooth, with the he varying by 2–4 nm on a lateral length scale of 50–100 Larger-scale scans (not shown) show the same beha\ the amplitude of roughness is only on the order of se\ nm, in contrast to sample I. The root-mean square slo estimated to be 5°–10°, implying (100) terrace width the range of 5–10 Å, assuming monatomic steps. The r phology is actually very similar to regions on samp between pyramids, which are more widely separated the edges of the sample than in the regions shown in l 2 and 3. The main change between samples I and II, tl fore, is suppression of pyramid and penetration twin mation. AFM scans of an as-polished (111) substrat vealed ridges and scratches from the polishing, with i in the range of 5–10 nm in height and a total height ation of less than 100 nm. The size of preexisting fea on the (100) substrate used to grow sample II were sumably similar in size. As the film thickness on samp ($2 \mu m$) is much greater than the probable size of prexi features, the morphology shown in Fig. 4 is probabl trinsic to the growth conditions, but a possible role o step density and roughness of the substrate cannot b cluded.

A large-scale three-dimensional image of sample shown in Fig. 6. The surface is decorated by bumps, : 100 nm wide by 1–5 nm high (note the very differen tical and horizontal scales in Fig. 6). We cannot d tively identify the bumps, but we believe them t adsorbed microdroplets of some kind, as they disapp after boiling sample III in sulfuric acid. Apart fror. bumps, the surface is extremely flat—large area . scans showed a total height variation of only 1–2 nm lateral distances of 1000–3000 nm. The root-mean-s slope is in the range of 0.1°, corresponding to (100) te widths of $\approx 20$ nm, again assuming monatomic step

A high-resolution image ($5 \times 5$ nm$^2$) of a porti sample III is shown in Fig. 7. Although individual : cannot be seen, evidence is seen for parallel lines sep; by 5.00–5.08 Å, as indicated by the white traces ad the upper portion of the figure. We believe that these :
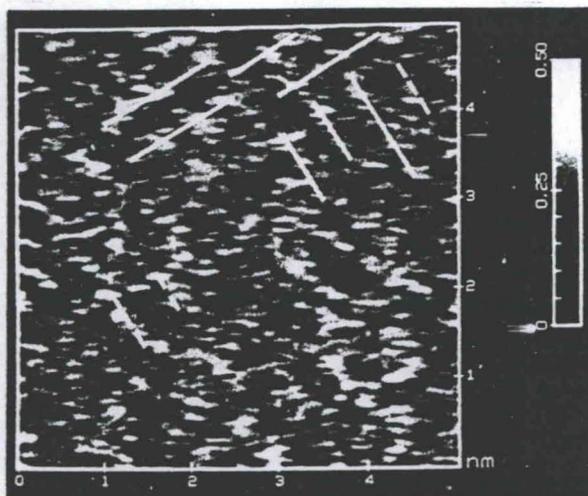
FIG. 7. High-resolution image of epitaxial (100) diamond film (sample III). White traces, separated by 5 Å, represent the location of (2×1) dimer rows.



FIG. 8. A top view model surface structure of the AFM image shown in Fig. 7. The shaded circles represent carbon atoms which are also bonded to hydrogen. The diameters of the carbon atoms diminish for each successive layer below the topmost one.

lines correspond to rows of dimerized surface carbon atoms which would have a theoretical separation of 5.04 Å, corresponding to a (2×1) reconstruction. Cross sections of the AFM image show that the uppermost rows are ≈0.9 Å higher than the rows rotated by 90° below and to the right, corresponding to a type-A monatomic step.[35] Similar (2×1) dimer rows and steps have been observed by STM on Si(100)[36,37] and Ge(100)[38] surfaces and, very recently, on a homoepitaxial (100) diamond film.[26] It is not clear why dimer rows cannot be seen in the rest of the image, but cross-sectional height measurements suggest that the upper and left-hand part of the image constitute the upper terrace and the remainder comprises the lower terrace. The structural model we propose for the AFM image shown in Fig. 7 is shown in Fig. 8. The shift in the rows on the upper terrace evident in Figs. 7 and 8 is an antiphase domain, where (2×1) domains with the surface atoms paired in the opposite way meet. Antiphase domains have also been observed in silicon epitaxy on Si(100)[37] at moderate temperatures. The (2×1) structure of Fig. 7 is presumably the monohydride, with one hydrogen atom per surface carbon atom.[39,40]

A three-dimensional view of the surface topography of sample IV is shown in Fig. 9. The (110)-oriented diamond film is very rough on the μm-mm scale, as observed by optical or electron microscopy.[9] A comparison of Figs. 9 and 3 shows that the morphology on the nm-μm scale is very different on the (110) and (100) films. The entire surface of the (110) film consists of hill-like features, ≈50–250 nm high and 100–800 nm wide, with no evidence of microfaceting. The total height variation in large-area scans was ≈500–1000 nm. The "hills" appear generally to be longer in one direction (near-vertical in Fig. 9) than in the orthogonal direction. The lateral dimensions of the hills and their diverse detailed structures indicates that the structures are real and not simply images of the tip. The orientation of the images with respect to the underlying
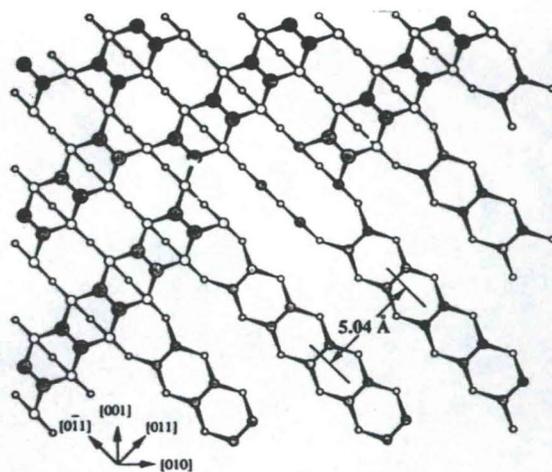
crystal lattice is unknown, but the existence of zig-zag chains of laterally bonded surface carbon atoms in the ⟨1̄10⟩ direction on ideal (110) surfaces suggests that this may be the "long" direction. Slopes as large as 46° were observed on the sides of the hills in the "narrow" direction, and slopes nearly as large are present in the "long" direction. The actual slopes may be somewhat larger due to the finite sharpness of the tip. The slopes are sufficiently large so that (100) and (111) planes are exposed locally on the surface: ⟨100⟩ lies 45° from ⟨110⟩ in the ⟨1̄10⟩ direction and ⟨111⟩ lies 35.3° from ⟨110⟩ in the ⟨001⟩ direction. The absence of any observable faceting on the (110)-oriented film is therefore noteworthy, as polycrystalline films are almost always dominated by (111) and/or (100) facets. The local morphology of the "hilltops" is extremely smooth, as is evident in the 5×5 nm² scan shown in Fig.
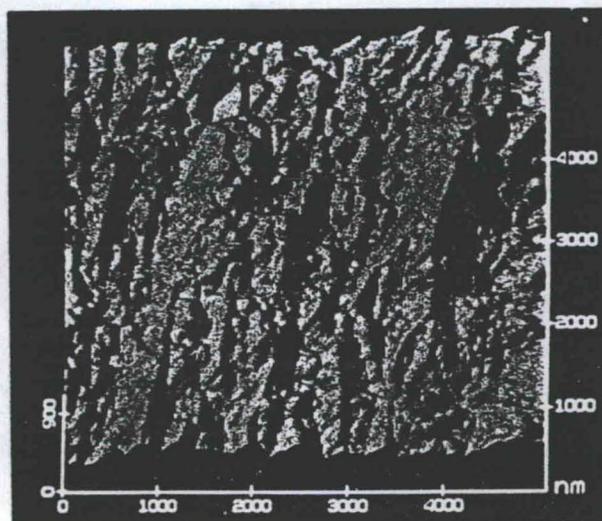


FIG. 9. Three-dimensional view of a representative portion of the (110) film surface (sample IV).
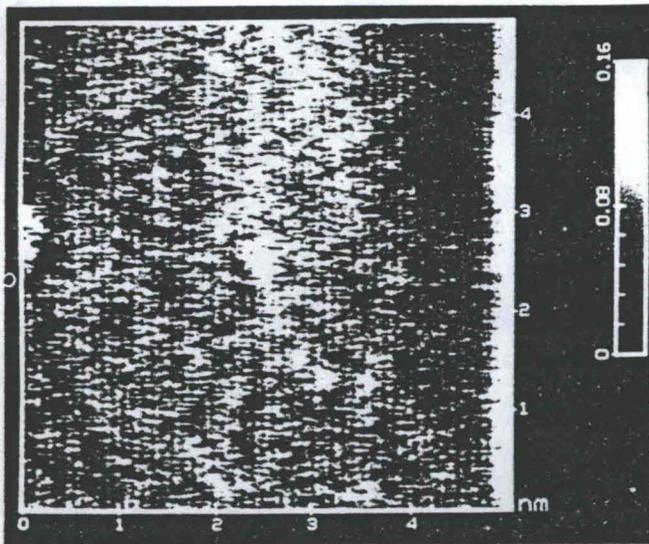
FIG. 10. High-resolution image of the (110) film surface, taken at the top of one of the "hills."

10. However, although the peak-to-peak roughness is less than 2 Å, comparable to sample III, no identifiable atomic features were observed.

Figure 11 is a grey-scale AFM image of sample V showing the intersection of two cracks formed at different times during the growth of the film. Larger area AFM images and optical micrographs of sample V showed cracks forming equilateral triangles and 60° parallelograms of various sizes. The six-fold symmetry of the cracks strongly suggests that the film is homoepitaxial, as spontaneous cleavage will occur on {111} planes, whose projections on the original (111) plane meet at 60° angles. Fracture took place after the film reached a critical thickness ($\approx 3.5 \mu m$)[9] and the sample was cooled and removed from the growth reactor for thickness measurements. An optical
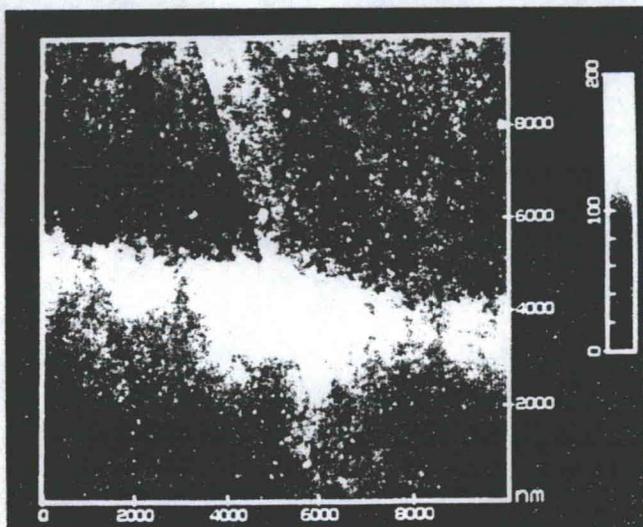


FIG. 11. AFM image of the (111) film surface (sample V) showing two intersecting cracks and a locally rough morphology.

micrograph of a similarly grown diamond (111) film l been reported previously.[9] Observation of interferei fringes in optical micrographs with the sample ligh from below and occasional missing plates on the surfi together indicate that fracture is accompanied by delai nation of the film. Cleavage from the substrate does i occur at the original interface, as might be expected nucleation was poor, as indicated by the roughness of s faces exposed by the occasional loss of plates of the fil The near-horizontal crack in Fig. 11 formed at an ea point in the growth of the film, with delamination a residual tensile stress causing the edges of the film to f upward. The sample was reinserted into the reactor a more diamond grown, resulting in "burial" of the cra and a more diffuse morphology. The sharpness of the si ond crack, running from the upper left to lower rig suggests that it formed immediately after the final fi growth step. The portion of the film to the right of t second crack flexed upward more than the left-hand pi tion, resulting in the asymmetric appearance. Cross si tions of the steps near cracks indicated typical step heigl of 20–200 nm.

The other noteworthy observation about the morph ogy of sample V is the degree of local roughness, both cli to and far away from cracks. Smaller area AFM sca taken near the centers of the triangular plates (i.e., from the cracks) show contiguous bumps with heights 10–50 nm and widths of 30–100 nm. Cross-sectional mi surements in regions far from any cracks revealed slopes high as 39°; actual slopes may be somewhat larger due convolution with the shape of the tip and the small late size of the features. However, no evidence of microfaceti was seen. We were unable to achieve a resolution higl than about 10 nm on this surface, perhaps due either erosion of the tip or instabilities in the motion of the across the surface.

## IV. DISCUSSION

A comparison of Figs. 2–7 demonstrates that grow conditions greatly affect the morphology of (100)-orient diamond films on the nm-$\mu$m scale, just as they are respc sible for well-documented variations in the micromet scale morphology of homoepitaxial diamond films[1-11] a diamond microcrystals and in the relative prevalence (100) and (111) facets in polycrystalline films.[41-50] T variable morphology is consistent with the disparate resu for (100)-oriented diamond growth reported by othe where (100) homoepitaxial films or (100) faces on mici crystals obtained under some conditions wi smooth[2(b),4,5,9,11,44,49,50] on the scale of the resolution of t instrument, whereas rough[1(b),2(b),3(b),8,46,48] or ev polycrystalline[1,3(b)] films were obtained under other con tions. While the present study demonstrates an effect surface temperature and hydrocarbon mole fraction, fi ther work will be necessary in order to precisely ident the aspects of the growth conditions responsible for speci features and the effects of the preexisting morphology a step density of the substrate and of the thickness of t film.

The morphological features of sample I are similar to features observed previously on CVD-grown diamond crystals or polycrystalline films on nondiamond substrates. Ledge formation during the growth of (100) faces of individual diamond crystals has been seen by a number of groups by scanning electron microscopy (SEM),[44-47] and smooth-sided pyramids have also been observed.[46] Although the orientation of the pyramids on sample I with respect to the crystallographic orientation of the substrate was not determined, the pyramid bases probably lie parallel to $\langle 01\bar{1}\rangle$ or $\langle 0\bar{1}1\rangle$, since these are the most stable orientations of steps on Si(100),[35-37] and steps in the $\langle 010 \rangle$ orientation, for example, would be atomically rough and there would be no driving force to keep the step edge straight. Although Okada et al.[47] observed evidence of ledge growth due to a screw dislocation, spiral ledges are not evident in any of our AFM images and are absent in other reports of ledge growth of (100)-oriented diamond films,[44-46] and therefore screw dislocations seem unlikely to play any important role in determining the morphology seen on sample I. Pyramids with and without ledges have been observed immediately adjacent to one another, both on sample I and on diamond microcrystals,[46] implying that growth can proceed along $\langle 100 \rangle$ or be tilted off—$\langle 100 \rangle$ by a few degrees by subtle differences in substrate and/or gas-phase conditions. To our awareness, penetration twins on (100) diamond films have been reported to date only by Clausing et al.[34] Further work, both experimental and theoretical, will be necessary in order to understand the precise factors responsible for the generation of pyramids and penetration twins.

The observation of essentially flat (100) surfaces following growth at higher substrate temperatures (Figs. 5–7), particularly at higher hydrocarbon flow rates, implies that growth occurs predominantly at steps, ledges, or kinks, or at least that extension of lattice planes occurs much faster than nucleation of a new layer. If this were not true, the surfaces would be much rougher on the nm scale due to nucleation and growth of new layers randomly across the surface. The fact that sample III is much flatter than sample II (terrace widths of $\approx 20$ and $\approx 0.7$ nm, respectively) implies that the ratio of the rate of step extension to that of nucleation of a new layer increases considerably as the hydrocarbon mole fraction and substrate temperature are increased.

Although the evidence for $(2 \times 1)$ dimer rows in Fig. 7 is admittedly less than compelling, we believe the features to be real, and similar observations of a $(2 \times 1)$ reconstruction on as-grown diamond (100) films by a number of other laboratories lead us to propose that in fact diamond (100) faces are predominantly covered by $(2 \times 1)$ dimer rows under CVD growth conditions. The structural model in Fig. 8 for the dimer rows in Fig. 7 is completely consistent with the AFM image: the spacing between the rows is correct, the cubic crystalline symmetry is correct, and the dimer rows on the terrace one atomic spacing higher are rotated by 90° as they should be. Generation of a spurious image by tip effects seems unlikely, as $Si_3N_4$ is not a cubic material and does not have structural features separated by

5 A. The STM images of CVD-grown diamond (100) by Tsuno et al.[26] are significantly clearer than Fig. 7, and their observations of dimer rows, type A and B single steps and type A double steps[35] seem beyond dispute. Tsuno et al.[26] did not report an antiphase domain of the type shown in Fig. 7, but such a structural feature is likely to be growth-condition dependent. Tsuno et al.[26] obtained further evidence of the $(2 \times 1)$ reconstruction by reflection high-energy electron diffraction (RHEED) following growth and transfer of the sample in air, and a similar observation was made by Thomas, Rudder, and Markunas[51] by low-energy electron diffraction (LEED), again following an air transfer. Finally, Sprang et al.[52] have also very recently reported observation of $(2 \times 1)$ dimer rows on a strongly (100)-textured polycrystalline diamond film by STM. The dimerized surface carbon atoms most likely exist in the monohydride configuration, with one hydrogen atom bonded to each atom in the dimer, since the structure is air-stable and samples are likely to be exposed to atomic hydrogen during the shutdown of the growth reactor.

The observation of $(2 \times 1)$-reconstructed diamond (100) surfaces by a number of workers, whose growth conditions presumably varied considerably, suggests that a dimerized surface structure dominates under CVD growth conditions rather than the more widely discussed $(1 \times 1)$:2H dihydride.[17(a),39] Theoretical support for this conclusion comes from the molecular mechanics calculations of Yang and D'Evelyn,[40,53] who found that the monohydride is the most stable high-symmetry phase over the temperature range of 298–1500 K, followed in stability by the clean surface, which also consists of $(2 \times 1)$-reconstructed dimers. The $(1 \times 1)$:2H dihydride was found to be thermodynamically unstable with respect to dehydrogenation due to extreme steric repulsion between nonbonded surface hydrogen atoms.[40,53] While observation of a surface structure after growth and air exposure does not prove that the structure was present under growth conditions, it is strongly suggestive, particularly when the structure is a stable one and its appearance is insensitive to the details of growth and reactor shutdown conditions, as evidenced by its observation in different laboratories. Since less-stable structures like the $(1 \times 1)$:2H full dihydride and the $(3 \times 1)$:1.33H partial dihydride[40,53] are favored at lower temperatures, if they did exist under growth conditions they would likely be stable as growth was quenched and the substrate was cooled. The fact that they have not been observed provides indirect evidence that they also do not exist in large concentrations under growth conditions and that the $(2 \times 1)$:H monohydride predominates, with clean $(2 \times 1)$ dimers perhaps also being important.

An additional argument for the existence of a $(2 \times 1)$ reconstruction on diamond (100) under growth condition follows from the observed smoothness of the film surface. The periodic bond chain (PBC) theory of Hartman and Perdok[54] relates the predicted smoothness and growth rates of particular crystal faces to the number of bonds each surface unit (atom) has with neighboring surface units, and successfully accounts for observed morphology of many types of crystals grown by a wide variety of methods

ods. However, application of the Hartman theory to the unreconstructed (100) surface of the diamond-structure lattice leads to the prediction of rough surfaces,[54] which is contradicted by the smoothness of (100)-oriented films not only of diamond but also of silicon, germanium, and gallium arsenide grown under wide-ranging conditions.[55] Giling and van Enckevort[55] showed that the contradiction could be resolved by assuming that $(2 \times 1)$ reconstructions are present during growth, with the dimer bonds supplying the missing surface bonds required by the PBC theory for smoothness. Their analysis assumes that the other unsatisfied valence on each (100) surface atom remains a dangling bond, whereas under diamond CVD conditions most dangling bonds are probably capped by chemisorbed hydrogen, forming the monohydride. However, the same argument applies as long as the step energy is positive, that is, formation of atomic steps costs energy, and therefore should be applicable to (100)-oriented diamond growth. On the other hand, the extreme steric hindrance in the $(1 \times 1)$:2H dihydride[40] is greatly reduced when dihydride units are not adjacent to one another,[40,53] suggesting that step formation on a dihydride-terminated surface would instead *lower* the surface energy. The negative step energy associated with the dihydride surface would predict extremely rough surfaces by the inverse of the argument of Giling and van Enckevort,[55] which is contradicted by the observed smoothness of the surfaces.

All CVD-grown, (110)-oriented homoepitaxial diamond film surfaces that have been characterized and reported to date have been rough on the $\mu$m scale.[2(b),3(b),4-10] (110) facets have only rarely been observed on CVD-grown diamond crystals.[49,50] However, the present results are the first to show their morphology on the nm scale. The observation of a high degree of corrugation, with local slopes as high as 45°, yet no microfaceting, is striking. The lack of faceting indicates that (110)-oriented growth is stable, in a sense, since the [100] and [111] orientations were exposed without becoming dominant. Only a distinct minority of the surface, however, has an orientation vicinal to $\langle 110 \rangle$. Figure 10 demonstrates that the film is extremely smooth on the nm scale, at least on top of the "hills," suggesting that the gross morphology is built up from one- or few-atom-high steps and kinks and that growth occurs preferentially at these low-coordination sites. The relatively random direction of the slopes provides fairly strong evidence for steps of widely varying orientation, even though they were not observed directly, which in turn implies that growth occurs at sites of varying local structure, not just at a single type of site.

Spontaneous fracture of (111)-oriented diamond films has been described by at least one other set of authors.[3] We have shown previously[9] that the cracking is a consequence of tensile stress, evidenced by a stress-shifted Raman peak in thin, (111)-oriented $^{13}$C diamond films which relaxed to the unstressed value as the film thickness was increased sufficiently (to $\approx 3.5$ $\mu$m) to induce spontaneous fracture. As noted above, fracture occurred after cooling and removal of the sample from the reactor. This suggests that the stress may actually by *thermal*, arising from unequal

thermal-expansion-coefficients of substrate and film, with the film having the larger value so that tensile stress ar upon cooling from the growth temperature. It is not cl whether the stress is isotropic across the film, but no dence was seen for splitting of the normally triply deg erate Raman peak and only a minor decrease in linewi occurred upon fracture.[9] The shift of the Raman peak quency can therefore be used to estimate the stress in fi prior to cracking. Using the reported pressure coefficien the Raman frequency, 2.75 cm$^{-1}$ GPa$^{-1}$,[56] the obser shift of $-5.1$ cm$^{-1}$ (Ref. 9) corresponds to a stress about 1.9 GPa. The film contracts by roughly 0.18% ative to the substrate upon fracture, using the bia Young's modulus of diamond of 1050 GPa,[57] which responds to a mean difference in thermal expansion co cients between film and substrate of $\approx 1.9 \times 10^{-6}$ K This value is a sizable fraction of the mean value of thermal expansion coefficient of diamond over the rang 25–966 °C, $\approx 3 \times 10^{-6}$ K$^{-1}$,[58] indicating that the mecl ical properties of the film are strongly perturbed. The ference also suggests that the modulus of the film is significantly different from bulk diamond, implying the calculations just given should be regarded as ro estimates only. The cause of the increased thermal exp sion coefficient in the (111) film is not clear, but Ra spectra indicate some incorporation of graphitic car into the film, and several authors have shown stacking-fault formation and twinning are ubiquitou (111)-oriented growth,[34,43(b),59-61] and either of these tors may be responsible.

Rough local morphologies have been reported on tually all the (111) diamond epilayers that have grown[1(c),3(b),4,8] and are also typically observed on ( facets of polycrystalline films and individual crystals.[4?] The detailed local structure is of obvious relevance to growth mechanism. The range of observed slopes or surface of sample V suggests that growth occurred at of varying structure, most likely steps. The short la range of the roughness ($\approx 30$–100 nm) provides ind support for proposals of propagation of defect structur [111] growth,[27,34,62] and the implication of growth pre inantly at non-(111)-like sites agrees with the calcula of Harris, Belton, and Blint,[63] who concluded that si hydrocarbon addition reactions to a flat (111) su could not account for observed growth rates. Howeve fairly amorphous "bump" structure observed in this is rather different than the triangular tiles and pits $\approx 1$ nm in size observed recently on (111) facets of ( grown diamond microcrystals by Hirabayashi and hara[50] using high-resolution SEM. The difference m due to some incorporation of graphitic carbon in our or, alternatively, to a sensitivity of the nanometer morphology in (111)-oriented growth to differences growth conditions, as we have shown occurs for ( oriented growth.

It seems appropriate to punctuate the above com on morphological similarities between homoepitaxia mond films and facets of diamond crystals with a c Existing evidence suggests that the submicrometer

phology of individual crystal faces on CVD-grown diamond microcrystals or polycrystalline films will normally *not* be directly analogous to the local structure of a homoepitaxial film of the same orientation. Several authors have reported differences in the local morphologies of the centers and edges of facets on CVD-grown diamond microcrystals.[49,50] In addition, the local morphology of diamond microcrystals has also been shown to depend on the substrate,[64,65] e.g., mechanically polished Mo, MoC, and diamond-like carbon.[65] These differences may result from perturbation of the gas-phase chemistry by the substrate, changing the local concentrations of the reactants. Such a perturbative effect has recently been demonstrated by Hsu,[12(g)] who showed that surface recombination of atomic hydrogen at the diamond surface strongly affects the gas-phase H concentration near the substrate, in agreement with the predictions of Goodwin and Gavillet.[66] The surface recombination rate of hydrogen, which is due to abstraction of surface hydrogen by incident atomic hydrogen, is almost certainly different on different substrates and may show significant differences on the different crystal faces of diamond. Given the importance of atomic hydrogen in determining the local concentration of $CH_3$,[12] the demonstrated importance of $CH_3$ in diamond CVD,[13,14] and the probable role of atomic hydrogen in driving surface reactions,[15-20] the effect just cited could well explain the observed differences in local morphology. Another possible cause or contributing factor may be local stress effects. Since (111)-oriented growth is accompanied by copious stacking-faults and twins,[4,34,43(b),59-61] whereas (100)-oriented growth is comparatively defect-free,[4,61] the edge regions of facets are likely to possess strain fields which are absent in the centers and affect the local surface morphology. Study of surface morphology on the nanometer-to-micrometer scale is therefore best done with *homoepitaxial* diamond films, where complications in the gas-phase chemistry and substrate properties are kept to a minimum.

Our results have implications for detailed diamond CVD growth models. As disparate growth models predict growth rates in reasonable agreement with experiment, it is clear that much more experimental input is necessary in order to discriminate between them and to establish the key steps in growth. We have demonstrated that growth conditions exert a significant effect on the nm-scale morphology, which is much more amenable to theoretical simulation than larger-scale structures. Growth models proposed to date focus on different crystal faces, including (100)-(1×1),[16(e),17(a)] (100)-(2×1),[16(e),20] (110),[17(c),18] flat (111),[15,17(b),19] and (111) with (100)-like[17(d)] or (110)-like[16] steps. We have argued above that a (2×1) reconstruction predominates on (100) surfaces under typical hot-filament CVD conditions and that growth occurs predominantly at sites of reduced coordination number, such as steps. Several authors have proposed microstructural effects associated with growth on diamond (110), including suggestions that (110) microfacets exist on faces of nominal (111)[49] or (100) orientation,[18] or that (110)-oriented growth is accompanied by (111)-microtwinning.[8]

The present results do not support these suggestions, as no evidence for micro- or nano-faceting was seen on (100) (110), or (111) epilayers, and the local orientation of ⟨ (110) epitaxial film was seen to vary smoothly from ⟨110⟩ to ⟨100⟩ and ⟨111⟩ and beyond. The development o ⟨110⟩ textures in polycrystalline diamond films appears t( be a simple consequence of growth rates in different crystallographic directions[34,61,67,68] requiring no special rol for the (110) face. Although detailed growth models hav not yet been applied to long-term simulation of atomic scale morphologies, it seems likely that the predictions o different models will differ qualitatively, offering an im proved basis for discriminating between them. Therefore, i seems reasonable to ask detailed growth models to mov beyond description of the initial stages of addition to th diamond lattice and estimation of growth rates to the pre diction of local surface morphologies of many-monolayer thick films for comparison with experiment.

## V. CONCLUSIONS AND SUMMARY

We have studied the surface topography on th nanometer-to-micrometer scale of homoepitaxial diamon films grown by hot-filament CVD conditions using atomic force microscopy. It is evident from the results that AFM can provide a wealth of information on the CVD growth o diamond films. Our principal observations may be summa rized as follows:

(i) (100) epitaxial films displayed a growth-condition dependent morphology: rough on the $\mu$m scale with pyra midal features and penetration twins at a substrate temper ature of 810 °C and low $CH_4$ flow rate; nearly atomicall smooth at 1000 °C and higher hydrocarbon flow rate.

(ii) Evidence for a dimer-type (2×1) reconstruction on smooth (100) surface was found.

(iii) A (110) epitaxial film was very rough ( > 100 nm) o the > 100 nm scale but nearly atomically smooth on th 0.5–5 nm scale and exhibited local slopes higher than 4( with no evidence of microfaceting.

(iv) A (111) epitaxial film with some graphitic conten fractured due to tensile stress and displayed ≈10–50 nr roughness on the 10–500 nm scale.

(v) The observed smoothness of the films on the nanom eter scale indicates that diamond growth is fastest at lov coordination-number sites.

[1](a) B. V. Derjaguin, B. V. Spitsyn, A. E. Aleksenko, A. E. Gorodetsl A. P. Zakharov, and R. I. Nazarova, Dokl. Akad. Nauk SSSR 21 1059 (1973) [Sov. Phys. Dokl. 18, 822 (1974)]; (b) B. V. Derjaguin, V. Spitsyn, A. E. Gorodetsky, A. P. Zakharov, L. L. Bouilov, and A.

5938    J. Appl. Phys., Vol. 71, No. 12, 15 June 1992

Sutcu *et al.*    59

Aleksenko, J. Cryst. Growth **31**, 44 (1975); (c) B. V. Spitsyn, L. L. Bouilov, and B. V. Derjaguin, *ibid.* **52**, 219 (1981).

[2] (a) N. Fujimori, T. Imai, and A. Doi, Vacuum **36**, 99 (1986); (b) H. Shiomi, K. Tanabe, Y. Nishibayashi, and N. Fujimori, Jpn. J. Appl. Phys. **29**, 34 (1990); (c) N. Fujimori, H. Nakahata, and T. Imai, *ibid.* **29**, 824 (1990).

[3] (a) H. Nakazawa, Y. Kanazawa, M. Kamo, and K. Osumi, Thin Solid Films, **151**, 199 (1987); (b) M. Kamo, H. Yurimoto, and Y. Sato, Appl. Surf. Sci. **33/34**, 553 (1988).

[4] M. Geis, Mater. Res. Soc. Symp. Proc. **162**, 15 (1990).

[5] A. R. Badzian, T. Badzian, X. H. Wang, and T. M. Hartnett, in *New Diamond Science and Technology*, edited by R. Messier, J. T. Glass, J. E. Butler, and R. Roy (Materials Research Society, Pittsburgh, PA, 1991), p. 549.

[6] K. Okano, Y. Akiba, T. Kurosu, M. Iida, and T. Nakamura, J. Cryst. Growth **99**, 1192 (1990).

[7] G. Janssen, W. J. P. van Enckevort, J. J. Schaminée, W. Vollenberg, L. J. Giling, and M. Seal, J. Cryst. Growth **104**, 752 (1990).

[8] J. F. DeNatale, A. B. Harker, and J. F. Flintoff, J. Appl. Phys. **69**, 6456 (1991).

[9] C. J. Chu, M. P. D'Evelyn, R. H. Hauge, and J. L. Margrave, J. Appl. Phys. **70**, 1695 (1991).

[10] K. A. Snail and L. M. Hanssen, J. Cryst. Growth **112**, 651 (1991).

[11] J. B. Posthill, R. A. Rudder, G. C. Hudson, D. P. Malta, G. G. Fountain, R. E. Thomas, R. J. Markunas, T. P. Humphreys, R. J. Nemanich, and D. R. Black, in *Diamond Materials*, edited by A. J. Purdes, J. C. Angus, R. F. Davis, B. M. Meyerson, K. E. Spear, and M. Yoder (The Electrochemical Society, Pennington, New Jersey, 1991), p. 274.

[12] (a) F. G. Celii and J. E. Butler, Annu. Rev. Phys. Chem. **42**, 643 (1991), and references therein; (b) S. J. Harris, A. M. Weiner, and T. A. Perry, Appl. Phys. Lett. **53**, 1605 (1988); (c) M. Frenklach, J. Appl. Phys. **65**, 5142 (1989); (d) S. J. Harris and A. M. Weiner, *ibid.* **67**, 6520 (1990); (e) C.-H. Wu, M. A. Tamor, T. J. Potter, and E. W. Kaiser, *ibid.* **68**, 4825 (1990); (f) D. G. Goodwin and G. G. Gavillet, *ibid.* **68**, 6393 (1990); (g) W. L. Hsu, Appl. Phys. Lett. **59**, 1427 (1991).

[13] (a) C. J. Chu, M. P. D'Evelyn, R. H. Hauge, and J. L. Margrave, J. Mater. Res. **5**, 2405 (1990); (b) M. P. D'Evelyn, C. J. Chu, R. H. Hauge, and J. L. Margrave, J. Appl. Phys. **71**, 1528 (1992).

[14] (a) L. R. Martin and M. W. Hill, J. Mater. Sci. Lett. **9**, 621 (1990); (b) S. J. Harris and L. R. Martin, J. Mater. Res. **5**, 2313 (1990).

[15] (a) M. Tsuda, M. Nakajima, and S. Oikawa, J. Am. Chem. Soc. **108**, 5780 (1986); (b) M. Tsuda, M. Nakajima, and S. Oikawa, Jpn. J. Appl. Phys. **26**, L527 (1987).

[16] (a) M. Frenklach and K. E. Spear, J. Mater. Res. **3**, 133 (1988); (b) D. Huang, M. Frenklach, and M. Maroncelli, J. Phys. Chem. **92**, 6379 (1988); (c) M. Frenklach and H. Wang, Phys. Rev. B **43**, 1520 (1991); (d) D. Huang and M. Frenklach, J. Phys. Chem. **95**, 3692 (1991); (e) D. Huang and M. Frenklach *ibid.* **96**, 1868 (1992).

[17] (a) S. J. Harris, Appl. Phys. Lett. **56**, 2298 (1990); (b) S. J. Harris, D. N. Belton, and R. J. Blint, J. Appl. Phys. **70**, 2654 (1991); (c) D. N. Belton and S. J. Harris, J. Chem. Phys. **96**, 2371 (1992); (d) S. J. Harris and D. N. Belton, Thin Solid Films (in press).

[18] W. A. Yarbrough, in *Diamond Optics IV*, edited by S. Holly and A. Feldman, Proc. SPIE **1534**, 90 (1991).

[19] P. Deák, J. Giber, and H. Oechsner, Surf. Sci. **250**, 287 (1991).

[20] B. J. Garrison E. J. Dawnkaski, D. Srivastava, and D. W. Brenner, Science **255**, 835 (1992).

[21] K. F. Turner, B. R. Stoner, L. Bergman, J. T. Glass, and R. J. Nemanich, J. Appl. Phys. **69**, 6400 (1991).

[22] H.-G. Busmann, H. Sprang, I. V. Hertel, W. Zimmermann-Edling, and H.-J. Güntherodt, Appl. Phys. Lett. **59**, 295 (1991).

[23] L. H. Robins, E. P. Whitenton, E. N. Farabaugh, and A. Feldman, in Ref. 5, p. 619.

[24] M. P. Everson, M. A. Tamor, and C. H. Wu, in Ref. 5, p. 613.

[25] A. W. Phelps and T. W. Owens, in Ref. 11, p. 502.

[26] T. Tsuno, T. Imai, Y. Nishibayashi, K. Hamada, and N. Fujimori, Jpn. J. Appl. Phys. **30**, 1063 (1991).

[27] J. C. Angus, Z. Li, M. Sunkara, R. Gat, A. B. Anderson, S. P. Mehandru, and M. W. Geis, in Ref. 11, p. 125.

[28] L. F. Sutcu, M. S. Thompson, C. J. Chu, R. H. Hauge, J. L. Margrave, and M. P. D'Evelyn, Appl. Phys. Lett. **60**, 1685 (1992).

[29] C. J. Chu, R. H. Hauge, J. L. Margrave, and M. P. D'Evelyn (unpublished).

[30] R. J. Nemanich, J. T. Glass, G. Lucovsky, and R. E. Shroder, J. V. Sci. Technol. A **6**, 1783 (1988).

[31] D. S. Knight and W. B. White, J. Mater. Res. **4**, 385 (1989).

[32] J. Wagner, M. Ramsteiner, Ch. Wild, and P. Koidl, Phys Rev. B 1817 (1989).

[33] For example, A. M. Cody and R. D. Cody, J. Cryst. Growth **83**, (1987), and references therein.

[34] R. E. Clausing, L. Heatherly, E. D. Specht, and K. L. More, in Re: p. 575.

[35] D. J. Chadi, Phys. Rev. Lett. **59**, 1691 (1987).

[36] R. J. Hamers, R. M. Tromp, and J. E. Demuth, Phys. Rev. B **34**, 5 (1986).

[37] R. J. Hamers, U. K. Kohler, and J. E. Demuth, J. Vac. Sci. Techno **8**, 195 (1990).

[38] J. A. Kubby, J. E. Griffith, R. S. Becker, and J. S. Vickers, Phys. F B **36**, 6079 (1987).

[39] A. V. Hamza, G. D. Kubiak, and R. H. Stulen, Surf. Sci. **237**, (1990).

[40] Y. L. Yang and M. P. D'Evelyn, J. Am. Chem. Soc. **114**, 2796 (19) 

[41] J. C. Angus and C. C. Hayman, Science **241**, 913 (1988).

[42] W. A. Yarbrough and R. Messier, Science **247**, 688 (1990).

[43] (a) S. Matsumoto, Y. Sato, M. Tsutsumi, and N. Setaka, J. Mater. **17**, 3106 (1982); (b) S. Matsumoto and Y. Matsui, *ibid.* **18**, 1 (1983).

[44] K. Kobashi, K. Nishimura, Y. Kawate, and T. Horiuchi, Phys. Re **38**, 4067 (1988).

[45] K. V. Ravi and A. Joshi, Appl. Phys. Lett. **58**, 246 (1991).

[46] H. Itoh, T. Nakamura, H. Iwahara, and H. Sakamoto, in Ref. 5, p. J. Cryst. Growth **108**, 647 (1991).

[47] K. Okada, S. Komatsu, S. Matsumoto, and Y. Moriyoshi, J. Cr Growth **108**, 416 (1991).

[48] S. J. Harris, A. M. Weiner, and T. A. Perry, J. Appl. Phys. **70**, 1 (1991).

[49] J. S. Kim, M. H. Kim, S. S. Park, and J. Y. Lee, J. Appl. Phys. **67**, : (1990).

[50] K. Hirabayashi and N. I. Kurihara, Jpn. J. Appl. Phys. **29**, L186 1901 (1990).

[51] R. E. Thomas, R. A. Rudder, and R. J. Markunas, in Ref. 11, p.

[52] H. Sprang, H.-G. Busmann, I. V. Hertel, W. Zimmermann-Edling, H.-J. Güntherodt, presentation at the Second European Conferenc Diamond, Diamond-like and Related Coatings (Nice, France, Sep ber 1991).

[53] Y. L. Yang and M. P. D'Evelyn, J. Vac. Sci. Technol. A (in pres:

[54] P. Hartman and W. G. Perdok, Acta Crystallogr. **8**, 49, 521 (1955 Hartman, in *Crystal Growth: An Introduction*, edited by P. Hart (North-Holland, Amsterdam, 1973), p. 367.

[55] L. J. Giling and W. J. P. van Enckevort, Surf. Sci. **161**, 567 (198:

[56] Mean of values reported by: (a) E. Whalley, A. Lavergne, and P. 7 Wong, Rev. Sci. Instrum. **47**, 845 (1976); (b) S. L. Sharma, H Mao, P. M. Bell, and J. A. Xu, J. Raman Spectrosc. **16**, 350 (1985): M. Hanfland, K. Syassen, S. Fahy, S. G. Louie, and M. L. Cohen, F Rev. B **31**, 6896 (1985); (d) H. Boppart, J. Van Straaten, and Silvera, *ibid.* **32**, 1423 (1985); (c) A. Tardieu, F. Cansell, and Petitet, J. Appl. Phys. **68**, 3243 (1990).

[57] (a) H. J. McSkimin, P. Andreatch, Jr., and P. Glynn, J. Appl. Phy: 985 (1972); (b) H. J. McSkimin and P. Andreatch, Jr., *ibid.* **43**, (1972); (c) M. H. Grimsditch and A. K. Ramdas, Phys. Rev. I 3139 (1975).

[58] G. A. Slack and S. F. Bartram, J. Appl. Phys. **46**, 89 (1975).

[59] B. E. Williams, J. T. Glass, R. F. Davis, and K. Kobashi, J. C Growth **99**, 1168 (1990).

[60] J. Narayan, J. Mater. Res. **5**, 2414 (1990).

[61] Z. L. Wang, J. Bentley, R. E. Clausing, L. Heatherly, and L. L. Ho in *Applications of Diamond Films and Related Materials*, edited t Tzeng, M. Yoshikawa, M. Murakawa, and A. Feldman (Elsevier, sterdam, 1991), p. 489.

[62] (a) J. C. Angus, R. W. Hoffman, and P. H. Schmidt, in *Proceedir: the First International Conference on New Diamond Science and ; nology* (KTK Scientific, Tokyo, 1991), p. 9; (b) J. C. Angus, I Buck, M. Sunkara, T. F. Groth, C. C. Hayman, and R. Gat, Bulletin, 38 (October 1989); (c) M. Sunkara, J. C. Angus, C. C. man, and F. A. Buck, Carbon **28**, 745 (1990).

[63] S. J. Harris, D. N. Belton, and R. J. Blint, J. Appl. Phys. **70**, (1991).

[64] K. Kobashi, K. Nishimura, K. Miyata, K. Kumagai, and A. Makaue, J. Mater. Res. 5, 2469 (1990).

[65] K. V. Ravi, C. A. Koch, H. S. Hu, and A. Joshi, J. Mater. Res. 5, 2356 (1990).

[66] D. G. Goodwin and G. G. Gavillet, in Ref. 5, p. 335.

[67] (a) Ch. Wild, N. Herres, and P. Koidl, J. Appl. Phys. 68, 973 (1990); (b) C. Wild, P. Koidl, N. Herres, W. Müller-Sebert, and T. Eckerman, in Ref. 11, p. 224.

[68] E. D. Specht, R. E. Clausing, and L. Heatherly, J. Mater. Res. 5, 2351 (1990).